RJC

RASĀYAN *J. Chem.*
Vol. 16 | No. 1 |376-384| January - March | 2023
ISSN: 0974-1496 | e-ISSN: 0976-0083 | CODEN: RJCABP
http://www.rasayanjournal.com
http://www.rasayanjournal.co.in

HYDROTHERMAL SYNTHESIS AND CHARACTERIZATION STUDIES OF NANO GRAPHENE OXIDE / COPPER OXIDE (CuO) NANOCOMPOSITES SUITABLE FOR SUPERCAPACITOR APPLICATIONS

M. Sappani Muthu[1,✉], P. Ajith[1], J. Agnes[1], M. S. Selvakumar[2], M. Presheth,[2] and D. Prem Anand[1]

[1]Materials Research Centre, Dept. of Physics, St. Xavier's College (Autonomous), Palayamkottai- 627002, Tamilnadu, India
[2]Department of Chemistry, St. Xavier's College (Autonomous), Palayamkottai- 627002, Tamilnadu, India
(Affiliated to Manonmaniam Sundaranar University, Abishekapatti 627012, Tirunelveli, Tamilnadu, India)
✉Corresponding Author: ts.tamil7594@gmail.com

ABSTRACT

The chemical properties of copper oxide (CuO) have made it an important material in the field of advanced technology for decades. The advantages of this material are its low cost, chemical stability, and remarkable electrochemical performance. The applications are found particularly in the fields of photovoltaic and energy storage. Growing energy supercapacitors have gotten a lot of interest because of their promising capacitance, availability, obvious electrochemical response, and ease of manufacture of copper oxides to address the high need for efficient electrochemical energy storage systems. This research describes a hydrothermal technique to produce GO/CuO nanocomposite for supercapacitor applications. XRD, FTIR, SEM, UV, and TGA, were used to evaluate the crystal nature, morphology, and chemical states of the produced GO/CuO nanocomposite, and electrochemical performance was tested using CV the manufactured nanocomposite materials as supercapacitor electrodes. The electrochemical results demonstrated that the GO/CuO nanocomposite is a good material for a supercapacitor electrode.

Keywords: Nano Graphene Oxide, Copper Oxide, Nanocomposite, Cyclic Voltammetry, Thermal Analysis, XRD.
RASĀYAN *J. Chem.*, Vol. 16, No.1, 2023

INTRODUCTION

Recent studies on practical energy storage systems have focused on the development of high-performance electrochemical energy devices such as batteries and supercapacitors. For long periods of time, they produce high power densities, short charging times, and excellent safety characteristics. Research has been extensively conducted on superconductors. Copper oxide (CuO) is a common element on Earth and one of the low-cost materials with a high capacitance that may be used in energy storage devices. Graphene oxide (GO) is one of the most significant graphene derivatives.[1] The oxygen functional groups in GO reveal a multilayer structure. Because of its unique surface features and layered structure, it may be thought of as a possible nano-sized building block for innovative materials with superior qualities.[2] Copper oxides are promising materials because of their low cost, availability, chemical stability, and environmental friendliness. Copper oxides were produced and deposited via anodization and electro-spun methods, resulting in specific capacitances of 212 and 620 f/g, respectively. Because of its efficiency, copper oxide has played a prominent role among them Supercapacitors must be built with electrical conductivity, structural flexibility, band gap, and charge carrier mobility in mind. Because of their technical perspective, nanocrystals have an intriguing reaction. Copper oxide (CuO) is one of these oxides being studied due to its unique properties. Solar energy conversion, lithium-ion batteries, Nanofluid, anodes in battery-solar cell superconducting materials, gas sensors, field effect transistors and field emitters, magnetic storage devices, photovoltaic devices, and other applications make CuO NPs an

http://doi.org/10.31788/RJC.2023.1618190

appealing material. Graphene, a very high-conductivity but low-capacitance active material, is used in conventional electrochemical double-layer capacitors (EDLcs). In general, supercapacitors are classified as pseudocapacitors or electrochemical double-layer capacitors based on the available electrochemical methods of energy storage for pseudocapacitors. In order to attain high power and energy density, it is important to have a high specific surface area, high electrical conductivity, and a quick diffusion process.[5-6] In order to improve the pseudocapacitive characteristics of plain copper oxide, the inclusion of additional transition metal oxides, has been explored; various works on the integration of Li in CuO for optical applications can be found in the literature. Magnetic application of Mn, CuO In converting and storing energy, supercapacitors, and pseudocapacitors (sodium-iron and lithium-ion batteries) are considered to be the most practical and active technologies. Among these technologies, the electrochemical supercapacitor, also known as the supercapacitor, has received Due to its fast charging and discharging capabilities, high power density, and long life span, the electrochemical supercapacitor is called an electro-double layer capacitor (EDLC). There are many carbon-based materials found in this application, including carbon nanotubes, graphene, and graphene oxide. This process is housed in a pseudo capacitor, which comprises conducting polymers and metal oxide and stores energy via a faradic redox reaction with the electrode material. Because of the significant volume expansion during cycling, the electrochemical performance of this material deteriorates.[7-8] CuO, which possesses high electrical conductivity and unique rate capabilities, was evenly distributed across the carbon matrices. Thermal stability has improved, which bodes well for usage in efficient electrochemical energy storage.[9]

EXPERIMENTAL

Material and Methods

Graphite flake powder (FG), sulphuric acid (H_2SO_4), potassium permanganate ($KMnO_4$), sodium nitrate ($NaNO_3$), hydrogen peroxide (H_2O_2), Hydrochloric acid (HCl), Ethanol, Copper Acetate $(CH_3COO)_2Cu.H_2O$.

Synthesis of Graphene Oxide (GO)

Graphite oxide (GO) was prepared by a modified Hummers process and the preparation is described in a typical procedure. Concentrated H_2SO_4 (70 mL) was added to the mixture of flake graphite (FG) powder (1.5 g), sodium nitrate (3.0 g), and $NaNO_3$ in the flask, then stirred in an ice bath for 45 minutes stir chilled. $KMnO_4$ (9.0 g) potassium permanganate was added very slowly and the temperature was kept below 293K. After stirring well in the ice bath for 2 hours, the mixture is placed in a water bath and kept warm at 308 K for 1 hour. The water (140 ml) was then added to the mixture, gradually increasing the temperature to 371 K and keeping it at this temperature for 1 hour. The reaction temperature was found to rise rapidly to 373 K with bubbling and the color changed to brown. Then the mixture of 30 ml H_2O_2 was added to the above solution and the color changed to yellow. To obtain GO, the solid mixture was separated by filtration and high-speed centrifugation (6000 rpm), rinsed with HCl solution and water, and then dried in a vacuum at 323 k for 96 hours.[10]

Synthesis of Graphene Oxide (GO)/ Copper Oxide (CuO) Nanocomposites

50 mg of GO was dispersed in 65 mL of ethanol by sonication for 3 hours. Then a calculated quantity of copper acetate was added to the solution such that the mass ratio between CuO and GO would be 1:1 with continued ultrasonication for one hour. The resultant suspension was sealed in a Teflon-lined autoclave with a capacity of 100 mL and was heated at 473K for 12 hours. The final product was filtered and dried in a vacuum at 323K for 24 hours. To have a comparative study, pure CuO and graphene sheets were made by the above method.[11]

RESULTS AND DISCUSSION

XRD

The Powder X-Ray diffraction analysis of the as-prepared Nano sample was carried out using a rigaku D/max-Ka diffractometer with a wavelength using molybdenum as the target material. The average crystalline size of the as-prepared nano sample was evaluated from the diffractogram using the Debye-Scherer formula $D=0.89\ \lambda/\beta \cos\theta$, where λ wavelength of the incident beam and β is the full width at half maximum and θ is the Braggs diffraction angle. As shown in Fig.-1(a), the average particle size was

found to be 21nm from the diffractogram several prominent peaks are 15.15º, 19.59º, 21.83º, 24.83º, 27.06º, 32.92º, 43.75º, 45.55º, 55.89º, these peaks agree well with the standard data of JCPDS file card no: 75-2078. The peaks at 21.51º and 27.06º are very intense these peaks uniformed the presence of graphite oxide nanoparticles with good interlayered structures. A peak at 2 θ = 27.06º is attributed to the oxygenated graphite. The peak at 55.89° disappears and was replaced by a peak at 45.55º. This is due to the chemical oxidation and exfoliation of the graphite. The XRD pattern confirms the nanographene oxide belongs to the tetragonal hausmannite crystal structure. As shown in Figure 1(b), the second layer shows Copper oxide (CuO) profiles from XRD. These peaks exactly corresponded to those of the monoclinic structure of CuO JCPDS card No: 05-0661, which includes diffraction peaks (110), (002), (111), (112), (202), and (020). This study found no additional impurities in CuO, indicating that the method produced very pure CuO. Crystallites of CuO measure 17.47 nm on average based on Scherer's equation. The XRD profiles of GO/CuO nanocomposite show GO with cubic phase as the dominant diffraction peak, while CuO exhibits the second peak. Results of XRD analysis demonstrate that GO and CuO coexist.[12]

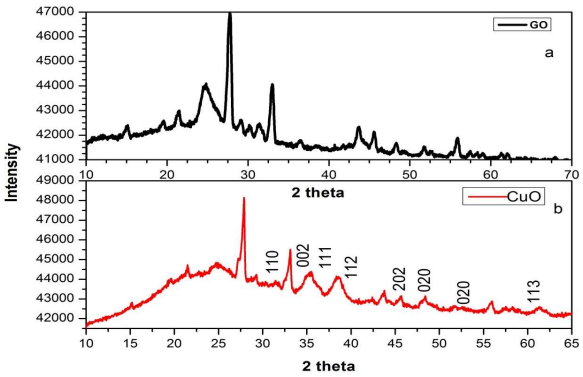

Fig.-1:(a) XRD Pattern of Nano Graphene Oxide. (b) Graphene Oxide / CuO nanocomposite

FTIR

Essentially, it involves obtaining the infrared spectra of infrared-absorbing solids, liquids, and gases, Analysis of an unknown mixture quantitatively through the determination of their absorption, emission, and photoconductivity. Approximately proportional to the amount of material present is the number of iterative peaks after oxidation. It appears that the GO produced exhibits a peak of 619 cm^{-1} in Fig.-2(a). This corresponds to the C-O bond showing that oxygen exists in the oxidation process, documenting the formation of functional groups. A peak in the range of 1571 cm^{-1} to 1111 cm^{-1} indicates that the C-C bond is still oxidized, while a peak in the range of 2925 cm^{-1} to 3416 cm^{-1} indicates the amount of water absorbed by GO. In part, this is because it creates a syrup that is jelly-like in appearance, OH absorbent substance contributes to the trace of H_2O molecules in this substance.

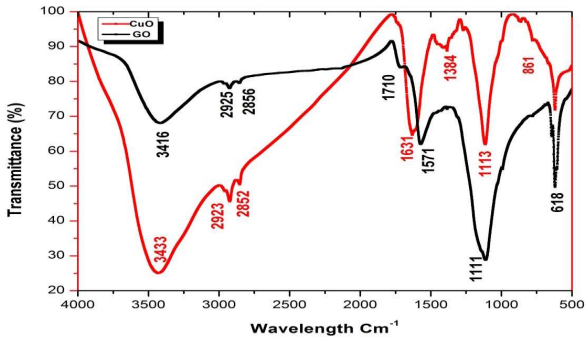

Fig.-2(a) FTIR Analysis of Nano Graphene Oxide (GO) (b) Nano Graphene Oxide / CuO Nanocomposite

Figure-2(b) shows FTIR spectrum of CuO/Nano graphene Oxide nanocomposite produced by hydrothermal method, with peaks in the 400-4000 cm^{-1} range. The appearance of peaks at 618 cm^{-1} verified the vibration of the CuO band, indicating that cuprous iron was oxidized to CuO by GO during the synthesis process. Furthermore, an OH-switching vibration occurred at 3433cm^{-1}. The presence of the

hydroxide group is shown by the vibrational spectra of CuO which records the spectrum at 2923 cm^{-1}. O-H bending vibrations paired with copper atoms may be responsible for the absorption peaks at 1631cm^{-1} and 1113 cm^{-1}. The Cu-O stretching modes are related to the two bromide absorption bonds, 618 and 500 cm^{-1}. The FTIR data indicates the existence of Cu-O as a consequence.[13-15]

SEM

SEM micrographs of CuO/graphene Nanosheets are shown in Fig.-3. The micrograph shows a granola-shaped spherical morphology with a width of 1µm. Graphene sheets are well connected with each other. This is an indication that the graphene oxide has been foliated during the preparation process. This may be due to the distorted graphene sheets when oxygen and other functional groups are attracted to the sheets of graphene oxide by copper oxide/graphene oxide nanocomposite connected with graphene oxide. This indicates that graphene sheets CuO overlapped each other. The surface is not within the nano range. Hence, it confirms that the particles are at the nanoscale.

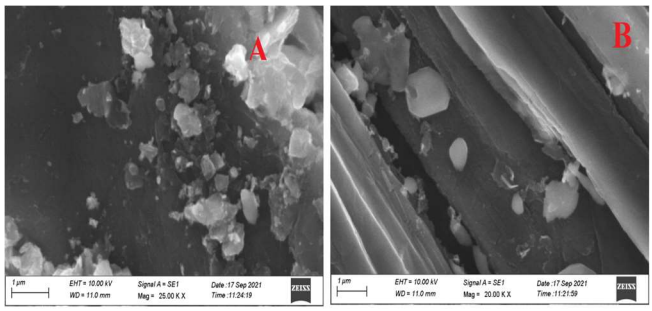

Fig.-3: SEM Morphology of Nano Graphene Oxide and CuO nanocomposite

UV

CuO nanoparticles are characterized by their ultraviolet-visible absorption spectrum. This curve shows the optical characterization of CuO nanoparticles. The Figure is shown in Fig.-4(a). A CuO nanoparticle's optical band gap energy (E_g) is calculated using Tauc's relation by $\alpha hv=(hv-E_g)/2$ is the absorption coefficient, V is the photon frequency, and hv is the incident photon energy. Based on whether the transition is direct or indirect, n can either take the value 1/2 or 2 to determine the type of electronic transition causing the absorption. For a direct transition spectrum of CuO NPs, the energy intercept of the plot of $(\alpha hv)^2$ vs hv yields E_g. Extrapolating the linear portion of the curve produces an energy intercept, which can be used to estimate the CuO NPs' energy band gap. There will be three intervals required to get $(\alpha hv)2 = 0$. This is much larger than the band gap of bulk CuO. Due to nanoparticles' decreased dimensionality and size, a strong blue shift is observed.

Absorption Coefficient

Describes how much light can be absorbed by a particular material thickness. Low absorption coefficients make it difficult to absorb light then the light is poorly absorbed and its absorption is also high. It depends on the material and also on the wavelength of the light that is being absorbed. The synthesized nano-graphene oxide/CuO nanocomposite shows maximum absorbance at 194 nm. So that it can absorb light wavelengths at 316nm more efficiently. Further, it was observed that the graph has an odd trend in which it decreases initially, becomes slightly more positive, and then straightens out again as shown in Fig.-4 (c). i) Nanocrystalline materials do not have defects, and they have an internal electric field, which is shown by this experiment, ii) an internal electric field of the material, absorption Coefficient $a=2.303*A/t$, A–absorbance (315nm),l-length of the cubit(1cm).

Skin Depth

The optical penetration depth of a substance and electromagnetic wave's depth of penetration may enter it. Skin depth $\delta={}^1/\alpha$,α– Absorption coefficient, as shown in Fig.-4 (d). It can be seen that skin depth increases up to 246 nm and then decreases. The minimum value of skin depth was approximately 308 nm and then began to climb until it reached its maximum at 387 nm. This demonstrates that electromagnetic radiation with a wavelength of around 398 nm is reaching the substance more deeply.

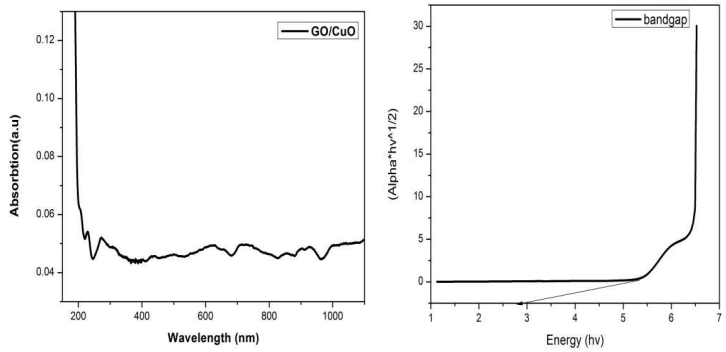

Fig.-4 (a) Absorbance and (b) Tauc's Plot GO/CuO Nano Composite

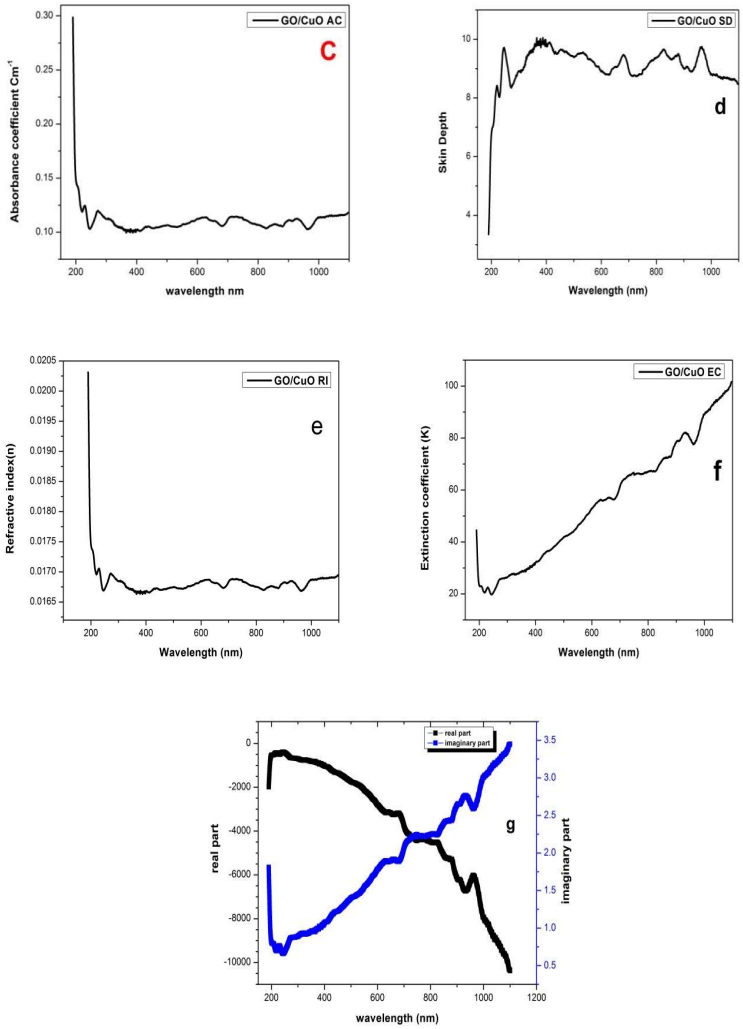

Fig.-4: (c) Absorption Coefficient, (d) Skin Depth, (e) Refractive Index, (f) Extinction Coefficient (g) Dielectric Constant

Refractive Index

The measurement of how light propagates through a substance; the greater the refractive index, the slower light will pass through the material, changing its direction; it is a crucial optical constant in the design of optical systems. It gives information on the local field, ii) polarization, and iii) the phase velocity of light. Figure-4 (e) This graph indicates that the Refractive index initially lowers and then grows to its highest value at 315 nm before returning to a constant or straight line.

Extinction Coefficient

The degree to which a chemical species or material absorbs light at a specific wavelength. It is determined by the produced material's structure and chemical makeup. The extinction coefficient is a measure of the absorption of electromagnetic radiation in a material and the loss through scattering. $K=a\lambda/4M$, α– Absorption Coefficient, λ is the Wavelength, from Fig.-4 (f) the extinction coefficient briefly decreases and then increases with increasing wavelength 244 nm it is increased after 890 nm it goes linear or says become constant.

Dielectric Constant

The calculation of the dielectric constant is used to find the permittivity and polarizability of a substance in conjunction with the density of states within the forbidden energy gap. The real part of the dielectric constant provides information about the speed of light that can be slowed down in the material. The imaginary part indicates the energy absorbed by an electric field due to dipole movement.

Dielectric Constant Real Part$A=\pi r^2=n^2-k^2$
Imaginary part $\varepsilon_i=2nk$
Refractive Index K–Extinction coefficient

Figure-4 (g) the fluctuation of the real and imaginary components of the dielectric constant have an opposing tendency, as shown by the Dielectric Constant of the produced sample. The greatest value of the real part is at 246 nm, indicating the most absorption, while the minimum value is at 1086 nm. Likewise, the maximum value of the imaginary part is at 1094 nm, indicating the highest absorption, while the minimum value is at 247 nm.

TGA/DTA

TGA analysis can be used to study chemical processes such as thermal decomposition, phase transitions, and oxidation and reduction. A TGA was performed on GO without damage, and it is shown in Fig.-5 (a) that the sample degrades in three steps. First, a good sample is one that demonstrates the melting point of untouched sample H_2O molecules; second, GO thermally dissolves with a higher weight loss than pure 600°C or 700°C; there is no endothermic peak before decomposition. Due to the large surface area of the amphora phase, GO melts at this temperature, despite almost completely decomposing before the 900°C point reaches thermal stability. Figure-5 (b) The TG-DTA curve of GO/CuO is shown. Nitrate is eliminated throughout the GO/CuO manufacturing process. The significant mass loss that began at about 200°C is due to GO/CuO decomposition, and mass loss from 200 to 400°C is approximately 5.85 percent. The mass loss above 400°C can be ascribed to CuO/GO phase production, and the mass loss between 700 and 800°C is around 9.33, with total disintegration of the residual composite at 800°C. a large exothermic peak at 453°C, implying that the oxidation process may remove oxygen vacancies from the system. The samples with a minor endothermic peak at 385°C, which corresponds to CuO/GO group breakdown, had better thermal stability. [13-16]

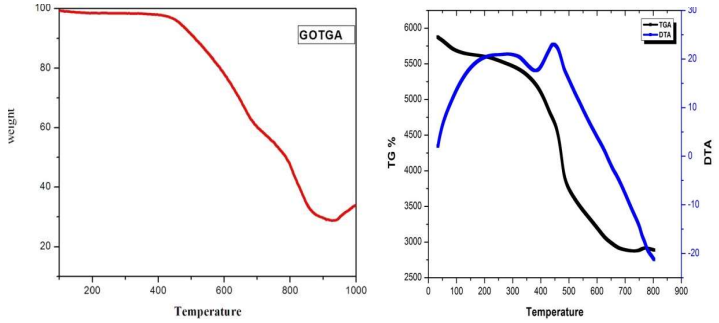

Fig.-5: Thermal Analyses of TGA/DTA of Nano Graphene Oxide and CuO Nanocomposite

Electrochemical Analysis

The electrochemical test was performed in a three-electrode system using a potential start at room temperature. We used a glassy carbon disc of diameter 5mm as the electrode. On the working electrode,

the prepared ink was dropped. The glassy carbon electrode was polished using powdered alumina of 0.3-micrometer thickness to obtain a smooth texture. Suddenly rise ultrasonically in a mixture of ethanol and water, followed by the addition of 5mg of the catalyst. The notion was used as the binding agent Graphite rod and mercury oxide are the counter and reference electrodes used for the experiments. The electrochemical activity of the as-prepared sample was studied using CV and LSV. The LSV was recorded to evaluate ORR offset potentials and kinetics. In addition to that K-L plot was drawn with different rotation speeds at a scanning speed of $5ms^{-1}$. CV was determined for a potential of 10000 cycles in an alkaline medium. The OH tolerance of the catalyst was determined with LSV at a scan speed of 5mV/sec. Rotating disc electrode experiments were performed to measure the percentage of peroxide. A total of 20ml of the catalyst clash was coated on a GC disc to set the RRDE as a working electrode and the thin was dried at room temperature.

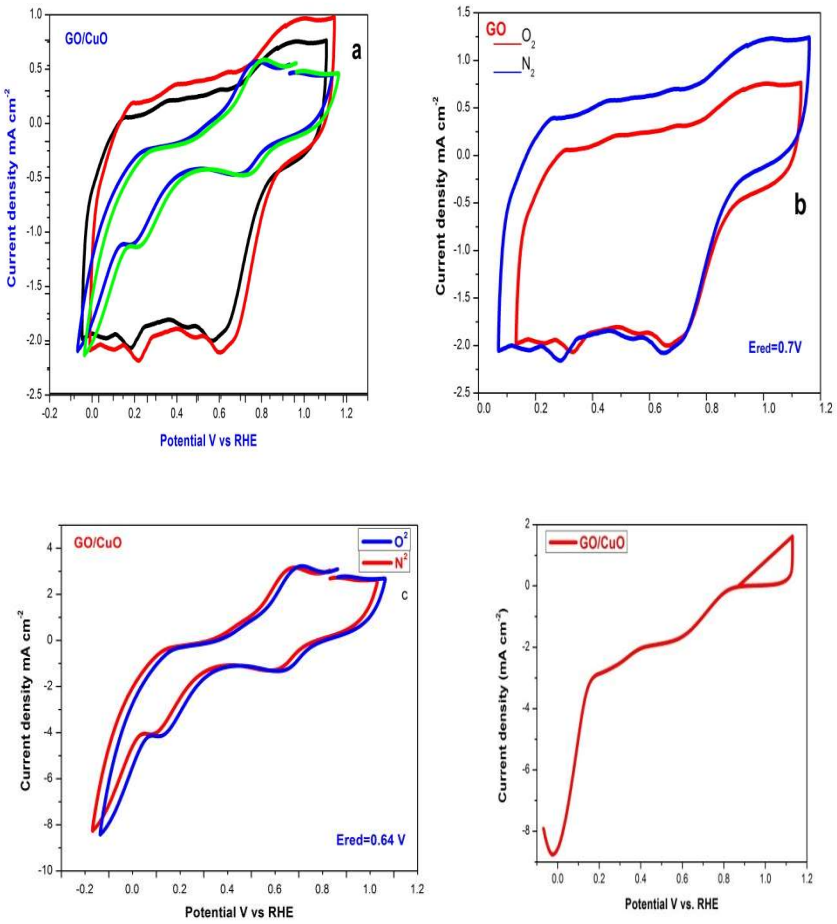

Fig.-6: (a) CV Curve of GO and GO/ CuO Composite Material, (b) CV Curve of Graphene Oxide, (c) GO/ CuO Nanocomposite CV Curve, (d) LSV of Composite Material GO/Cuo 1600 Cycle.

Three electrodes were used for the comparison of the electrochemical properties of GO/CuO nanocomposite. Additionally, CuO and GO were examined in terms of their electrochemical properties. As shown in Fig.-6 (c), the CV curves of the bare GO/CuO nanocomposite are plotted. As a result, CV measurements were performed on electrodes in the potential range of -0.2V to 1.2V. As shown in Fig.-6 (a), the CV curve of bare GO shows a rectangular shape without noticeable redox peaks. It is pseudo-capacitance that determines the capacitive behavior of GO nanosphere electrodes. In Fig.-6 a, an active electrode made of pristine CuO is illustrated with CV diagrams. All CV curves showed a pair of redox peaks at a 5 mV sampling rate over the -0.2 to 1.2 V voltage range, implying a comparable pseudocapacitive response and significant rate capability. In addition, the redox peak current ranges become larger as the scan sweep has increased. In addition, the cathodic peak shifted to a negative (−Ve)

potential as the resistance decreased and the ion and electron transfer rates increased. CuO electrode material morphology and chemical composition for reversible faradaic redox reactions and redox reactions resulting in KOH (potassium hydroxide) electrolytes could be closely correlated with the strong peaks. Figure-6. (b) appears to be CV plots of GO/CuO nanocomposites at a sampling rate of 5 mV/s. A composite electrode's CV curve exhibits relatively clear redox peaks, which can be attributed to the typical pseudocapacitive performance of a GO electrode.[16-19] The specific capacitance of the prepared sample is calculated using the provided formula. Cp = A/2mk (V_2-V_1), where A is the area with units inside the curve. The active material mass is m, the CV (50) sampling rate in volts per second is k, and the CV potential window is (V_2-V_1) (0.99).In the table, the specific capacity was calculated in Table-6.1.

Table-6.1: Specific Capacitance of Graphene Oxide. Graphene Oxide/Copper Oxide Nanocomposites

Sample	Saturated Solution	Area	Specific Capacitance F/g
Graphene Oxide (GO)	O2	0.0615978	615.978
Graphene Oxide (GO)	N2	0.0423410	423.410
Copper oxide (CuO)	O2	0.1424173	142.417
Copper oxide (CuO)	N2	0.0287512	287.512

A relation is used to measure the specific capacitance values of the GO/CuO nanocomposite. The GO/CuO electrodes' measured specific capacitance values are much larger than their individual compounds of bare GO and CuO electrode material. The increased specific capacity of the GO/CuO electrode is due to spherical GO nanoparticles that are tightly coiled on the surface of CuO nanoparticles, resulting in composites with a larger surface area.

Table-6.2: Comparative Study GO /CuO Nanocomposites of Supercapacitor with Various Methods and Nanostructure

Compounds	Method	Nanostructures	Electrolyte	Specific capacitance	Reference
CuO/MnO_2	Hydrothermal	Diatom	1 M Na_2 SO_4	240 F/g at 0.5 Ag^{-1}	16
MnO_2/NiO	Hydrothermal	Spherical	1 M KOH	247 F/g at 0.5 A/g	17
CuO/ Co_3O_4	Hydrothermal	Nano sheet	5 M KOH	246 F/g at (A/g)	19
MnO_2/CuO	Hydrothermal	Spherical	1M KOH	279.12 F/g at 0.5 A/g	20
GO/CuO	Hydrothermal	Nano sheet	1 M KOH	287.51 F/g at 0.5A/g	**Present work**

In conclusion, the specific capacitance performance comparisons of GO/CuO nanocomposites fabricated in the electrode material in the current work demonstrated better cycle performance than some previously reported works[20] (Table-6.2).

CONCLUSION

A graphene oxide /CuO_4 nanocomposite was successfully synthesized by a hydrothermal process. The results obtained from XRD, FTIR, SEM, UV, TGA, and Raman, CV showed that CuO nanoparticles were deposited on graphene. XRD confirmed the purity of the crystalline nature of the sample. The average nanocomposite size was found to be 17.47 nm. These functional groups were confirmed by FTIR spectra. SEM images show the uniform distribution of CuO nanoparticles on the graphene surface. The Raman spectrum is frequently used to characterize the D and G peaks. They rise following the electrochemical reduction of CuO, as well as a shift in the position of the D and G peaks. CV study was electrochemical properties specific capacitance value calculated in the GO/CuO composite is 287.51 F/g at 0.5 A/g.

ACKNOWLEDGEMENTS

The authors would like to thank the research which was supported and guided by Dr. Akhila Kumar sagu. CSIR principal scientist and Dr. Mageshkumar SPO, CSIR Chennai Tharamani complex Chennai, for their constant support and encouragement. The authors are very grateful for the constant support provided by Rev. Dr. S. Mariadoss S.J, the principal of St. Xavier's College, Palayamkottai, and Rev. Dr. Alphonse Manickam S.J, the secretary of St. Xavier's College, Palayamkottai.

CONFLICT OF INTERESTS

The authors have no conflicts of interest to declare. All co-authors have agreed with the contents of the manuscript and there is no financial interest to report.

AUTHOR CONTRIBUTIONS

All the authors contributed significantly to this manuscript, participated in reviewing/editing, and approved the final draft for publication. The ORCID ids of all the authors are given below:

M.Sappani Muthu http:/orcid.org/;0000-0003-3882-2547
D. Prem Anand http:/orcid.org/;0000-0002-2488-6884
P.Ajith http:/orcid.org/;0000-0003-2231-365X
J.Agnes http:/orcid.org/; 0000-0003-1866-4617
Selvakumar http:/orcid.org/;0000-0002-5744-8020
M. Presheth http:/orcid.org/; 0000-0003-3882-2547

REFERENCES

1. S. Sagadevan, Z. Zaman Chowdhury, A. Hawa, R.F. Rafique, *Journal of Experimental Nanoscience*, **13(1),** 284(2018), https://doi.org/10.1080/17458080.2018.1542512
2. M. Zhai, A. Li, and J. Hu, *Journal of Royal Society Chemistry Advances*, **10(60)**, 36554(2020), https://doi.org/10.1039/D0RA06758J
3. S.K. Shinde, D.P. Dubal, G.S. Ghodake, P. Gomez-Romero, S. Kim, V.J. Fulari, *Journal of Royal Society Chemistry Advances*, **5(39)**, 30478(2015), https://doi.org/10.1039/C5RA01093D
4. S.K. Shinde, D.P. Dubal, G.S. Ghodake, and V. Fulari, *Journal of Royal Society Chemistry Advances*, **5(6),** 4443(2015), https://doi.org/10.1039/c4ra11164h
5. A. Aljaafari, N. Parveen, F. Ahmad, M. Alam, S.A. Ansari, *Journal* of Scientific *Reports*, **9(1),** 1(2019), https://doi.org/10.1038/s41598-019-45557-6
6. S.M. Pawar, J. Kim, A. Inamdar, H. Woo, Y. Jo, B.S. Pawar, and H. Im, *Journal of Scientific Reports*, **6(1)**, 1(2016), https://doi.org/10.1038/srep21310
7. M. Hu, R. Cheng, H. Zhang, Q.H. Yang, *Journal of Nanoscale*, **12(2)**, 763(2020), https://doi.org/10.1039/C9NR08960H
8. B. Paulchamy, G. Arthi, B.D. Lignesh, *Journal of Nanomaterial Nanotechnology*, **6(1)**, 253(2015), https://doi.org/10.4172/2157-7439.1000253
9. N.I. Zaaba, K.L. Foo, U. Hashim, and C.H. Voon, *Journal of Procedia Engineering*, **184,** 469(2017), https://doi.org/10.1016/j.proeng.2017.04.118
10. H. Zheng, K.R. Roy, M. Gao, Y. Pan, X. Cai, and R. Li, *Journal of Applied Nano Science*, **13(10)**, 11488(2019), https://doi.org/10.1021/acsnano.9b04970
11. S. Akula, andA. K. Sahu, *Journal of Applied Materials and Interfaces*, **12(10)**, 11438(2020), https://doi.org/10.1021/acsami.9b18790
12. L. Yang, J. Shui, L. Du, Y. Shao, J. Liu, L. Dai, and Z. Hu, *Journal of Advanced Materials*, **31(13)**, 1804799(2019), https://doi.org/10.1002/adma.201804799
13. M.P. Kumar, M. Raju, A. Arunchander, S. Selvaraj, G. Kalita, T.N. Narayanan, and D.K. Pattanayak, *Journal of The Electrochemical Society*, **163(8)**, F848 (2016), https://doi.org/10.1149/2.0541608jes
14. Y. Zhang, W. Guo, T.X. Zheng, Y.X. Zhang, and X. Fan, *Journal of Applied Surface Science*, **427**, 1158(2018), https://doi.org/10.1016/j.apsusc.2017.09.064
15. K. M.Racik, K. Guruprasad, M. Mahendiran, J. Madhavan, T. Maiyalagan, M.V. Raj, *Journal of Materials Science: Materials in Electronics*, **30(5)**, 5222(2019), https://doi.org/10.1007/s10854-019-00821-3
16. S. Ramesh, A. Kathalingam, K. Karuppasamy, H.S. Kim, H.S. Kim, *Journal of Composites Part B: Engineering,* **166**, 74(2019), https://doi.org/10.1016/j.compositesb.2018.11.116
17. K.M. Racik, A. Manikandan, M. Mahendiran, P. Prabakaran, J. Madhavan, M.V. Raj, *Journal of Physica E: Low-dimensional Systems and Nanostructures*, **119**,114(2020), https://doi.org/10.1016/j.physe.2020.114033

[RJC- 8190/2022]